

Experimental observation of Type-II Weyl points and Fermi arcs in phononic crystal

Boyang Xie¹, Hui Liu¹, Hua Cheng^{1,3,*}, Zhengyou
Liu², Shuqi Chen^{1,3,4,†} and Jianguo Tian^{1,3,4}

¹*The Key Laboratory of Weak Light Nonlinear Photonics, Ministry of Education,
School of Physics and TEDA Institute of Applied Physics,
Nankai University, Tianjin 300071, China*

²*Key Laboratory of Artificial Micro- and Nanostructures of
Ministry of Education and School of Physics and Technology,
Wuhan University, Wuhan 430072, China*

³*The collaborative Innovation Center of Extreme Optics,
Shanxi University, Taiyuan, Shanxi 030006, China and*

⁴*Renewable Energy Conversion and Storage Center,
Nankai University, Tianjin 300071, China*

(Dated: January 13, 2019)

FROM TYPE-II TO TYPE-I WEYL POINT

We start from the tight-binding model proposed by Xiao *et. al.* [1]. The Hamiltonian of the system can be written as

$$H(\mathbf{k}) = \begin{pmatrix} \varepsilon_a + 2t_a \cos(k_z h) + t_c f(k_z h) & t_n \beta \\ (t_n \beta)^* & \varepsilon_b + 2t_b \cos(k_z h) + t_c f(-k_z h) \end{pmatrix}, \quad (1)$$

where

$$\beta = \exp(-ik_y a) + 2 \cos(\sqrt{3}k_x a/2) \exp(ik_y a/2),$$

$$f(k_z h) = 2 \cos(\sqrt{3}k_x a - k_z h) + 4 \cos(3k_y a/2) \cos(\sqrt{3}k_x a/2 + k_z h),$$

ε_a and ε_b represent the sublattice on-site energy. t_a , t_b are the interlayer non-chiral hopping, t_c is the interlayer chiral hopping, and t_n is the intralayer hopping. t_a , t_b , t_c , t_n are real and can be positive or negative for different bands. The Hamiltonian can also be written in the Pauli matrix form

$$H(\mathbf{k}) = d_0 I + d_x \sigma_x + d_y \sigma_y + d_z \sigma_z, \quad (2)$$

where

$$d_0 = \frac{\varepsilon_a + \varepsilon_b}{2} + (t_a + t_b) \cos(k_z h) + t_c \left[2 \cos(\sqrt{3}k_x a) \cos(k_z h) + 4 \cos\left(\frac{3k_y a}{2}\right) \cos\left(\frac{\sqrt{3}k_x a}{2}\right) \cos(k_z h) \right],$$

$$d_x = \cos(k_y a) + 2 \cos\left(\frac{\sqrt{3}k_x a}{2}\right) \cos\left(\frac{k_y a}{2}\right),$$

$$d_y = \sin(k_y a) - 2 \cos\left(\frac{\sqrt{3}k_x a}{2}\right) \sin\left(\frac{k_y a}{2}\right),$$

$$d_z = \frac{\varepsilon_a - \varepsilon_b}{2} + (t_a - t_b) \cos(k_z h) + t_c \left[2 \sin(\sqrt{3}k_x a) \sin(k_z h) - 4 \cos\left(\frac{3k_y a}{2}\right) \sin\left(\frac{\sqrt{3}k_x a}{2}\right) \sin(k_z h) \right].$$

The Weyl point can only exist along $KH(K'H')$ lines [$k_x = 4\pi/(3\sqrt{3}a), k_y = 0$ for KH] of the Brillouin zone (BZ) where the off-diagonal terms vanish. The band dispersion along KH is $E_1 = \varepsilon_b + 2t_b \cos(k_z h) + 6t_c \sin(k_z h - \pi/6)$ and $E_2 = \varepsilon_a + 2t_a \cos(k_z h) - 6t_c \sin(k_z h + \pi/6)$. Here we set $\varepsilon_a = \varepsilon_b$ (the $\varepsilon_a \neq \varepsilon_b$ case can be solved numerically). For structures with unequaled interlayer hopping term t_b and without chiral coupling ($t_c = 0$), we get type-II Weyl points when t_a and t_b are both positive or negative, otherwise we get type-I Weyl points. For the lowest two bands of our structure, we have $t_a < t_b < 0$ thus type-II Weyl points are achieved. When we gradually increase the chiral coupling t_c ($t_c < 0$ for the lowest

two bands), the type II Weyl points will finally turn into type I Weyl points. The k_z position of Weyl points can be solved by

$$\frac{t_a - t_b}{3t_c} = \frac{\cos(2\pi/3 + k_z h) - \cos(2\pi/3 - k_z h)}{\cos(k_z h)}. \quad (3)$$

At \bar{K} point [$k_x = 4\pi/(3\sqrt{3}a)$, $k_y = 0$], the positions of the Weyl point 1 (WP1) and Weyl point 2 (WP2) are $k_z(\text{WP1}) = -k_z(\text{WP2}) = k_{z0}$ for $t_c = 0$, and $0 < k_z(\text{WP1}) < k_{z0} < -k_z(\text{WP2}) < \pi/h$ for $t_c < 0$, where $k_{z0} = \pi/2h$ for $\varepsilon_a = \varepsilon_b$. From the dispersion at Weyl points, the turning point of type-II to type-I is

$$t_c = \frac{1}{18}(-t_a + t_b - \sqrt{t_a^2 + 22t_a t_b - 23t_b^2}). (t_a < t_b < 0, t_c < 0) \quad (4)$$

The corresponding phase diagram is shown in Fig. S2. The hopping strength can be tuned by changing the radius of the connecting tubes in acoustic systems. In the real acoustic systems, the position of Weyl points slightly shifts as the connecting tubes changes the on-site energy ε_a and ε_b . Although the tight-binding model cannot strictly describe the whole band dispersion, it can predict the band behavior, which is very useful in guiding the design of acoustic systems. The fitting results of the tight-binding model are shown in Fig. S1, where the relation between energy and frequency is $E \propto \omega^2$. The red circles and blue squares are from the simulation in the main text. The fitting parameters are $\varepsilon_a = 3.58$, $\varepsilon_b = 3.60$, $t_a = -0.55$, $t_b = -0.31$ and $t_c = -0.034$ in arbitrary unit.

THE CHIRALITY OF WEYL POINTS

The effective Hamiltonian around the Weyl point can be written into the general form [2]

$$H(\delta\mathbf{k}) = \sum \delta k_i v_{ij} \sigma_j, i, j \in \{x, y, z\}. \quad (5)$$

where v_{ij} are the group velocities and σ_j are the Pauli matrices. At \bar{K} point [$k_x = 4\pi/(3\sqrt{3}a)$, $k_y = 0$] the group velocity matrix is

$$v_{ij} = \begin{pmatrix} -3at_n/2 & 0 & 0 \\ 0 & 3at_n/2 & 0 \\ 0 & 0 & -h(t_a - t_b) \sin(k_z h) - 3\sqrt{3}ht_c \cos(k_z h) \end{pmatrix} \quad (6)$$

for $t_a < t_b < 0$ and $t_c \leq 0$, the chiralities (topological charges) are $c = \text{sgn}[\det(v_{ij})] = -1$ for WP1 and $c = +1$ for WP2, respectively.

TYPE-II WEYL PHONONIC CRYSTAL WITHOUT CHIRAL COUPLING

The schematic of phononic crystal without chiral coupling is shown in Fig. S3a. The geometric parameters are the same as the chiral structure. As this system still has mirror symmetry with respect to the y - z plane, the Weyl points of opposite charges are in the same k_z planes in the reciprocal space. Therefore, the net charge in the horizontal light green plane in Fig. S3b is zero and the Weyl points share the same degenerate frequency as shown in Fig. S3c. The Weyl points lie in \bar{K} and \bar{K}' points with $k_z = \pm 0.56\pi/h$ at $f = 9525$ Hz. The band structures in two-dimensional (2D) BZ planes $k_z = 0$ and $k_z = 0.56\pi/h$ are shown in Fig. S3d,e. Although the type-II Weyl points can exist without chiral coupling, the one-way surface acoustic waves (SAWs) can not exist at XZ and YZ surfaces because the topological charge of Weyl points cancel out through projection to the surfaces. The Weyl points also have the same frequency which means the SAWs are hard to be observed in the experiment. Here we compare the simulation results of surface states with [Fig. S4a,c] or without chiral coupling [Fig. S4b,d]. The field distribution in Fig. S4b is clearly a bulk state, which is apparently different from the SAW in Fig. S4a. The XZ surface bands in the chiral phononic crystal at $k_z = 0.6\pi/h$ plane are shown in Fig. S4c, where the SAWs propagating along XZ1 or XZ2 surface are denoted with green solid lines or dashed lines, respectively. The XZ surface bands in the non-chiral phononic crystal at $k_z = 0.56\pi/h$ are shown in Fig. S4d. No topological surface states are found in $k_z = 0.56\pi/h$ or other k_z planes.

DIRECT OBSERVATION OF THE SAWS

We demonstrate the existence of the Fermi arc-like surface states associated with the type-II Weyl points. To probe for surface states, we put a point-like sound source at the top of XZ1 surface to stimulate the $-k_z$ part of the surface states. Figure S5a shows the pressure field distribution of sound travelling from the XZ1 to the YZ1 surface at Fermi frequency 9600 Hz. No clear reflection signal is observed near the interface, unlike the conventional wave response to an interface. The sound is still coupled to the bulk modes, whether the frequency is between the Weyl points or not, which is exactly as expected for the type-II Weyl points. The pressure field distributions are shown in Fig. S5b-e for different

layers, indicating that a large amount of energy penetrates into the bulk while the SAWs are still hold in the surfaces. The signal reduces from intrinsic material absorption of air and scattering into bulk states. This measurement of robust propagation of a surface wave across the corner serves as a direct observation of the topological SAWs.

EXPERIMENT METHODS

A loudspeaker is used as sound source in the experiment measurements. The loudspeaker (diameter = 15 mm) is placed inside the sample at the center of the bottom layer for bulk states excitations. For surface states measurements, a sub-wavelength headphone (diameter = 5.7 mm) is used for sound excitations. The headphone is placed at the center of the corresponding surfaces with rigid boundaries. The sound sources are motivated by a broadband pulse. For the measurement of acoustic fields, a sub-wavelength microphone (diameter = 6.35 mm, B&K Type 4961) attached to the tip of a stainless-steel rod (diameter = 4 mm) is inserted into the sample through the space between the plates. Another identical microphone is fixed which serves as the phase reference. The acoustic signal is analyzed by a multi-analyzer system (B&K Type 3560B), with which both the amplitude and phase of the wave are extracted. The frequency spectrum for each point is obtained by averaging 110 FFT (Fast Fourier Transformation) results within 9.5 seconds. The scanning is performed by a stage moving in three directions. According to Nyquist-Shannon sampling theorem, a sufficient sampling rate (Fs) to map out the Brillouin zone is no less than one sample per period. The steps of the stage are 10.0 mm ($Fs_x = 2.2$), 19.1 mm ($Fs_y = 2$) and 17.3 mm ($Fs_z = 1$) in the x , y and z directions, respectively. The bulk and surface dispersions of the acoustic system are obtained by Fourier transforming the measured fields. The resolutions of Fourier transform along x , y and z direction are $0.037 \times 2\pi/\sqrt{3}a$, $0.069 \times 2\pi/3a$ and $0.069\pi/h$, respectively, which are restricted by the number of lattice periods. The measured pressure fields distribution is normalized by the source spectrum.

* hcheng@nankai.edu.cn

† schen@nankai.edu.cn

- [1] Meng Xiao, Wen-Jie Chen, Wen-Yu He, and C. T. Chan, Synthetic gauge flux and weyl points in acoustic systems. *Nat. Phys.* **11**, 920 (2015).
- [2] Ling Lu, Liang Fu, John D. Joannopoulos, and Marin Soljačić, Weyl points and line nodes in gyroid photonic crystals. *Nat. Photonics* **7**, 294 (2013).

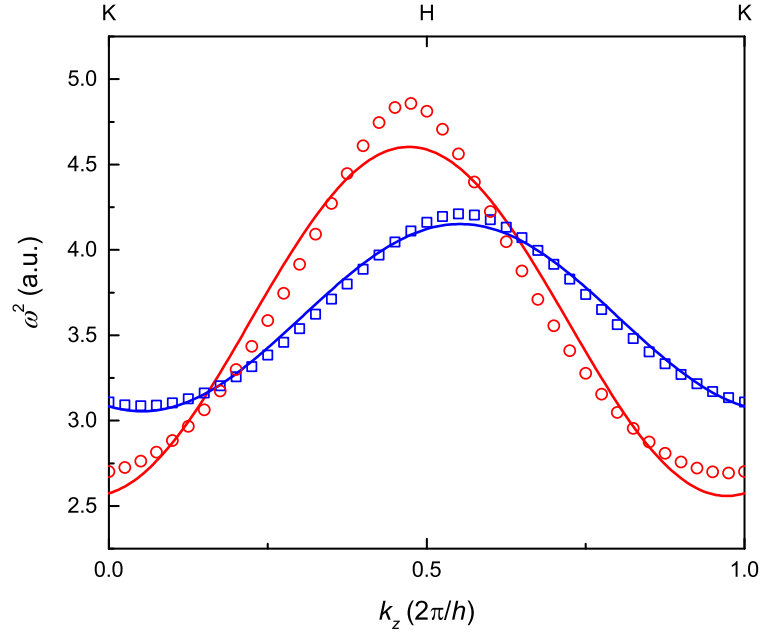


FIG. S1. The fitting results of the tight-binding model. The red circles and blue squares are the simulation results. The corresponding fitting results are in solid lines. The fitting parameters are $\varepsilon_a = 3.58$, $\varepsilon_b = 3.60$, $t_a = -0.55$, $t_b = -0.31$ and $t_c = -0.034$ in arbitrary unit.

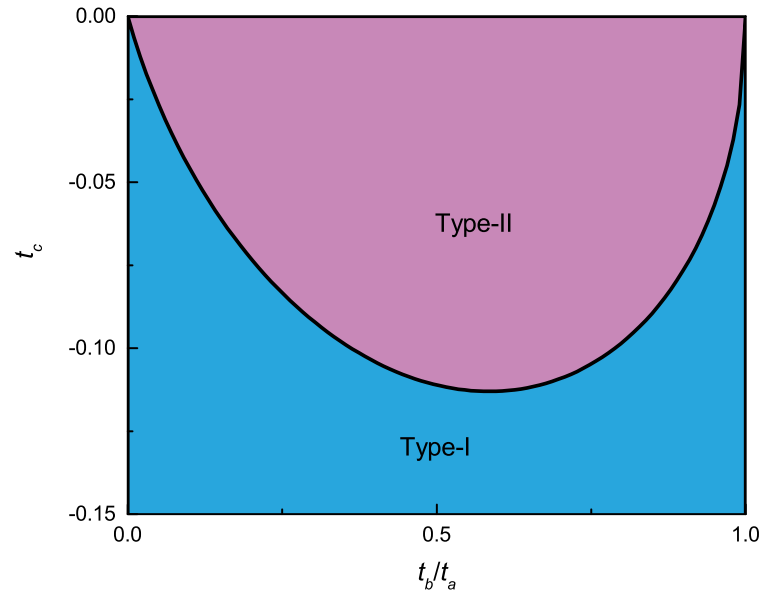


FIG. S2. Phase diagram of the Weyl phononic crystal with $\varepsilon_a = \varepsilon_b$.

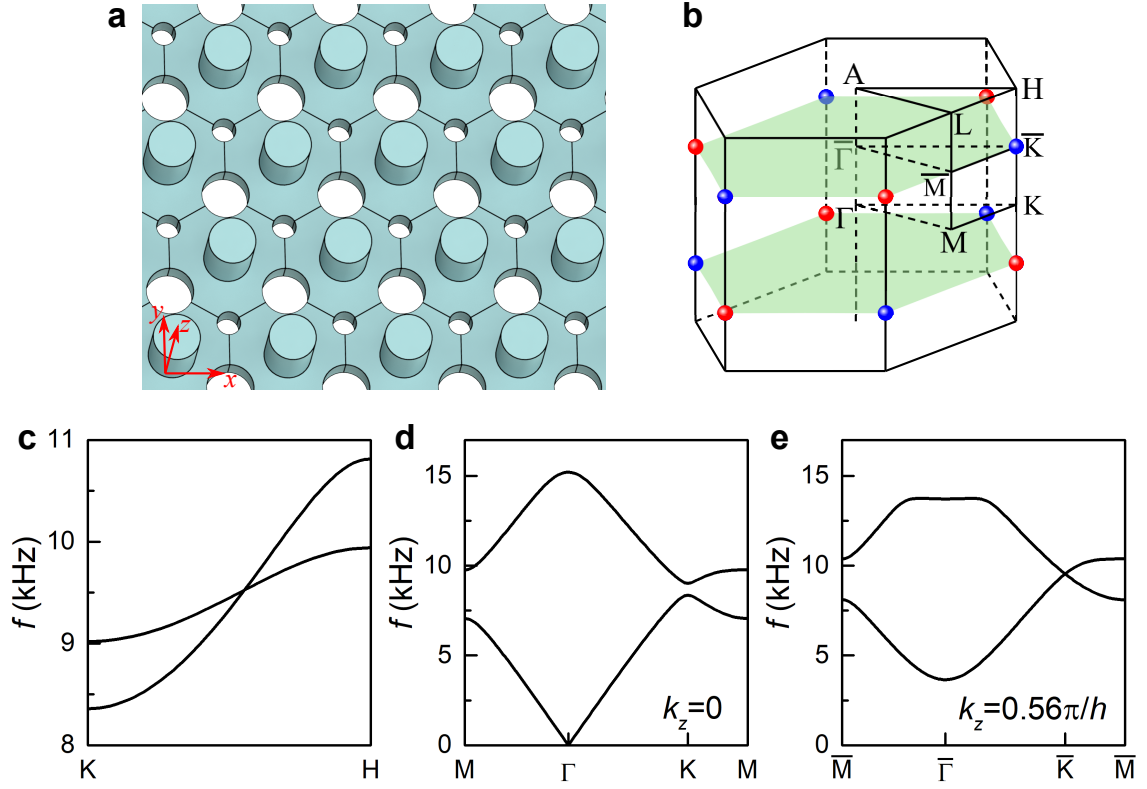


FIG. S3. (a) The schematic of the non-chiral type-II Weyl phononic crystal. (b) The first bulk BZ of the Weyl phononic crystal. The colored spheres label Weyl points with different topological charges. (c-e) The band structures along the high symmetry lines (c) in KH direction and (d,e) 2D BZ planes.

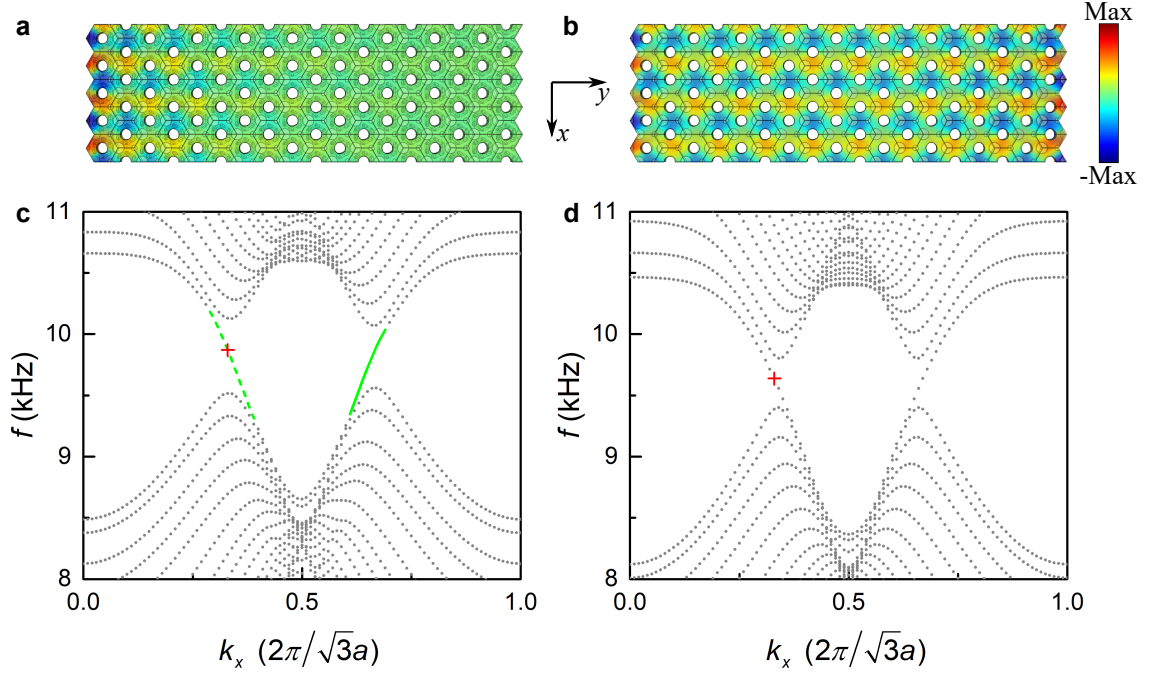


FIG. S4. XZ surface states of the phononic crystal (a, c) with interlayer chiral coupling, (b, d) without interlayer chiral coupling. (a, b) Pressure eigenfield distribution. (c, d) Surface band dispersion. The Bloch vectors are $k_x = 0.33 \times 2\pi/\sqrt{3}a$, $k_z = 0.6\pi/h$ for (a) and $k_x = 0.33 \times 2\pi/\sqrt{3}a$, $k_z = 0.56\pi/h$ for (b), which are denoted with red cross in (c) and (d), respectively.

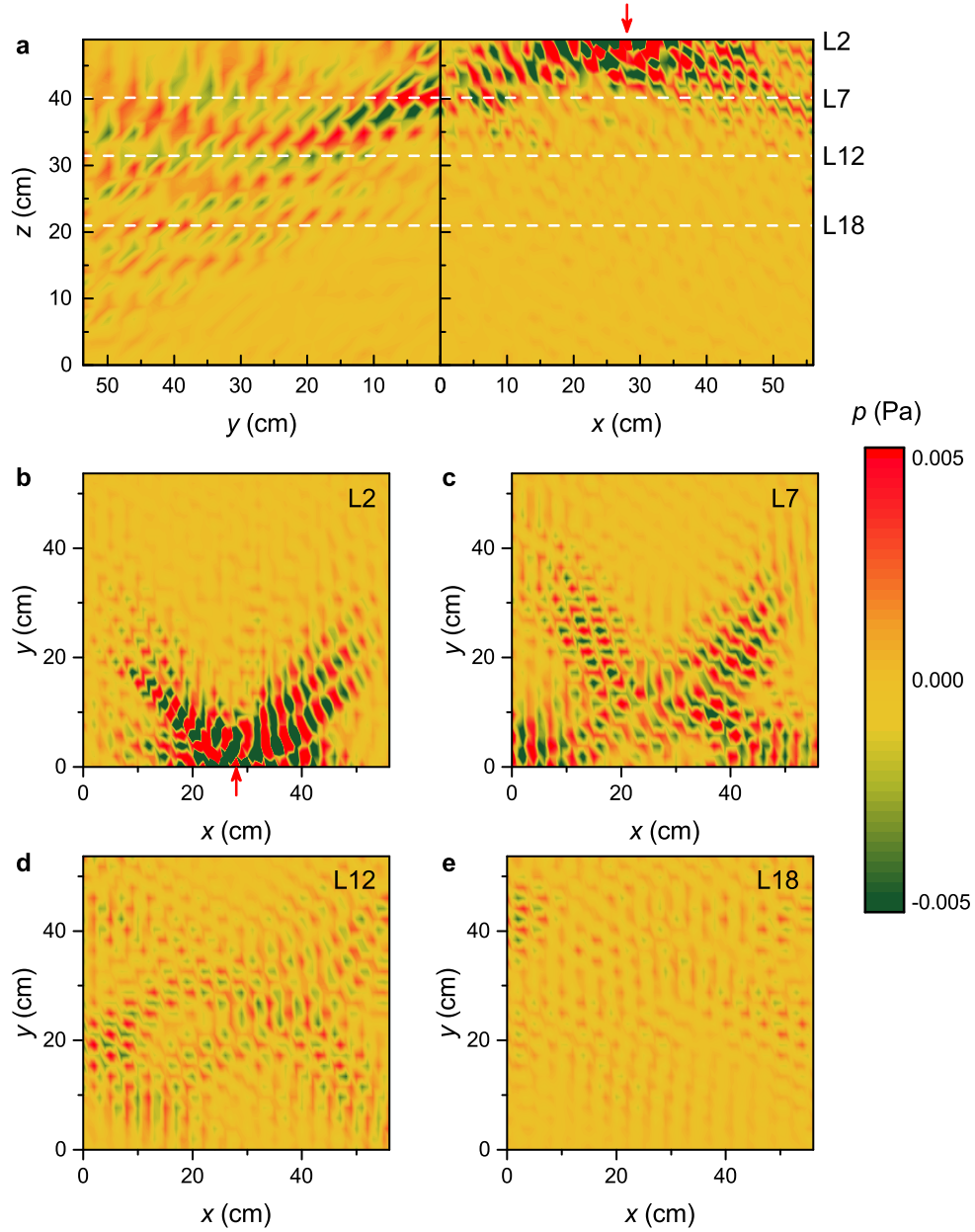


FIG. S5. Direct observation of Fermi arc-like surface acoustic waves. (a) Pressure field distribution of acoustic surface waves travelling from the XZ1 to the YZ1 surface. (b-e) Field distribution of different layers at (b) layer 2, (c) layer 7, (d) layer 12 and (e) layer 18. The sound source is placed at the center of the uppermost layer in XZ1 surface, denoted as the red arrow. The Fermi frequency is 9600 Hz.